nature communications

Article

https://doi.org/10.1038/s41467-024-53781-6

Chlorine isotopes constrain a major drawdown of the Mediterranean Sea during the Messinian Salinity Crisis

Received: 15 February 2024

Accepted: 17 October 2024

Published online: 18 November 2024

Check for updates

G. Aloisi[1] ✉, J. Moneron[2,3,4], L. Guibourdenche[1], A. Camerlenghi[5], I. Gavrieli[2], G. Bardoux[1], P. Agrinier[1], R. Ebner[6] & Z. Gvirtzman[2,3]

Hydrological restriction from the Atlantic Ocean transformed the Mediterranean Sea into a giant saline basin during the Messinian Salinity Crisis (5.97–5.33 million years ago). It is still unclear if the deposition of nearly one million km^3 of evaporite salts during this event was triggered by a major (≥1 km) evaporative drawdown, or if it took place in a brine-filled Mediterranean connected to the Atlantic. Here we present evidence for a two-phase accumulation of the Mediterranean salt layer based on the chlorine stable isotope composition of halite. During the first phase, lasting approximately 35 kyr, halite deposition occurred only in the eastern Mediterranean, triggered by the restriction of Mediterranean outflow to the Atlantic, in an otherwise brine-filled Mediterranean basin. During the second phase, halite accumulation occurred across the entire Mediterranean, driven by a rapid (<10 kyr) evaporative drawdown event during which sea-level dropped 1.7–2.1 km and ~ 0.85 km in the eastern and western Mediterranean, respectively. During this extreme drawdown event, the eastern Mediterranean basin lost up to 83% of its water volume, and large parts of its margins were desiccated, while its deep Ionian and Herodotus sub-basins remained filled with >1 km-deep brine.

Today, more freshwater is extracted from the Mediterranean Sea by evaporation than is added by continental runoff[1]. Blocking the net import of Atlantic Ocean waters through the Gibraltar sill would result in a Mediterranean sea level fall at a rate of about 0.5 m yr^{-1} (ref. 2). During the Messinian Salinity Crisis (MSC), the deposition of nearly one million km^3 of evaporite salts[3,4] (mainly gypsum, $CaSO_4.2H_2O$, and halite, NaCl) is a testimony of highly restricted hydrological exchange with the Atlantic Ocean. Whether or not evaporite deposition was accompanied by a major (≥1 km) sea level drawdown, however, is still debated. Estimates of the magnitude of the base-level fall during the MSC rely on geological indicators such as deeply incised canyons onland[5–9], widespread erosional surfaces on the margins[10–13] and in the basins[14–16] and evaporite facies from drilled cores[17–20]. However, these indicators are not interpreted unequivocally[21–24] and drawdown estimates range from ~ 200 m to ~ 2 km[9,11,14,21,25–27]. Existing hydro-chemical models cannot solve the controversy because they show that the complete MSC halite body can be deposited in scenarios that include periods of Mediterranean isolation and sea level drawdown[28], but also in scenarios involving exclusively a partially restricted, brine-filled Mediterranean[9,10,29].

We use the chlorine stable isotope composition of halite to estimate the volumetric halite precipitation rate in the Mediterranean basins during the MSC. Compared to other geochemical tracers such as strontium isotopes[30,31], chloride has the advantage of being a major constituent of halite and, for all practical purposes, is derived solely from inflowing seawater. Laboratory contamination issues are

[1]Université Paris Cité, Institut de Physique du Globe de Paris, CNRS, Paris, France. [2]The Geological Survey of Israel, Jerusalem, Israel. [3]Institute of Earth Sciences, Hebrew University, Jerusalem, Israel. [4]University of Oxford, Department of Earth Sciences, Oxford, UK. [5]National Institute of Oceanography and Applied Geophysics - OGS, Trieste, Italy. [6]Utrecht University, Department of Earth Sciences, Utrecht, The Netherlands. ✉e-mail: aloisi@ipgp.fr

https://doi.org/10.1038/s41467-024-53781-6

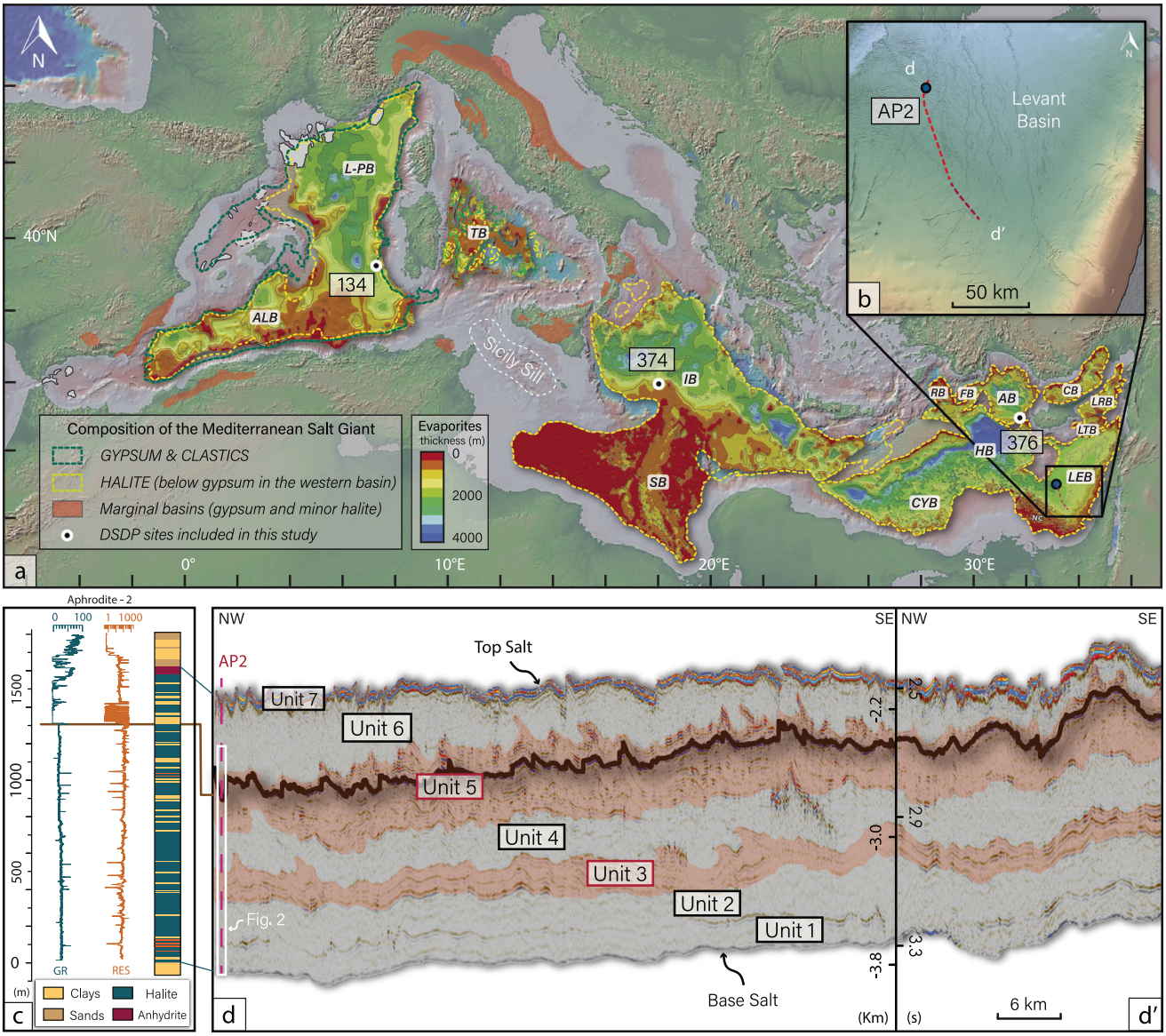

Fig. 1 | The Messinian Salt Giant of the Mediterranean sea. a Study area showing data and on-land and offshore Messinian evaporite thickness distribution[4] over a Mediterranean Basin map (background relief and bathymetry maps taken from https://www.geomapapp.org/). Chloride isotope data included in this work comes from the hydrocarbon industry well Aphrodite (AP2) located in the Levantine basin (eastern Mediterranean) and from Deep Sea Drilling Project (DSDP) sites 134 (western Mediterranean), 374 (Ionian Basin, eastern Mediterranean) and 376 (Florence rise, eastern Mediterranean). **b** location of the seismic section (red dashed line) shown in **d**. **c** Petrophysics and associated lithologic log of the Aphrodite well. GR-Gamma Ray (graph ranges between 0 – left - and 100 API) and RES-Resistivity (graph ranges between 0 – left - and 1000 Ωm; logarithmic scale) logs; **d** Composite seismic section (d-d') in the Levantine basin showing the Messinian evaporites composed of seven seismo-stratigraphic units[34]. Notes: in **a**, symbols are as follows: RB, Rhodes Basin; FB, Finike Basin; AB, Antalya Basin; CB, Cilicia Basin; LRB, Larnaca Basin; LTB, Latakia Basin; LEB, Levant Basin; HB, Herodotus Basin; CYB, Cyrenaica Basin; SB, Sirte Basin; IB Ionian Basin; TB, Tyrrhenian Basin; L-PB, Liguro-Provençal Basin; ALB, Algerian Basin; in the lithological log of **c**, orange layers represent clastic inclusions. Black horizon in seismic section of d is a high-amplitude continuous reflection corresponding to a layer of clastics encased in halite; in **d**, vertical distance is in km below sea level.

also minimal for this reason. At the basis of our approach is the chloride isotope reservoir effect which results from the preferential incorporation of the heavy isotope ^{37}Cl (as opposed to the lighter isotope ^{35}Cl) into precipitating halite[32]. The extent of the isotope reservoir effect depends on the balance between the rate of halite precipitation, which tends to decrease the $^{37}Cl/^{35}Cl$ ratio of dissolved chloride, and the rate of addition of dissolved chloride from the Atlantic Ocean, that tends to push Mediterranean $^{37}Cl/^{35}Cl$ towards heavier global ocean values. The faster the precipitation, the stronger the ^{37}Cl-depletion of the precipitating halite. Evaporative drawdown of a halite-saturated water column[33] results in very high rates of halite precipitation, and in the most extreme dissolved Cl, and thus halite, ^{37}Cl-depletion.

Results and discussion

Chloride isotope composition of halite

We analyzed 60 drill cuttings from the Aphrodite well (Levantine basin, eastern Mediterranean) starting from the onset of halite precipitation and spanning a thickness of 1393 m upcore (Fig. 1). All analytical results are presented in Supplementary Tables 1–3. In the Levantine basin, the Messinian evaporite package is divided into the following seven seismic subunits[34]. Four transparent units are composed mainly of halite. Two intercalated, highly reflective units are composed of halite with a higher, albeit laterally variable, clay content. A seventh unit is composed of a mixture of anhydrite, clays and sands, separated from the underlying units by the Intra-Messinian Truncation Surface (IMTS, interpreted as a dissolution surface)[34] (Fig. 1d). Bulk XRD analyses of

https://doi.org/10.1038/s41467-024-53781-6

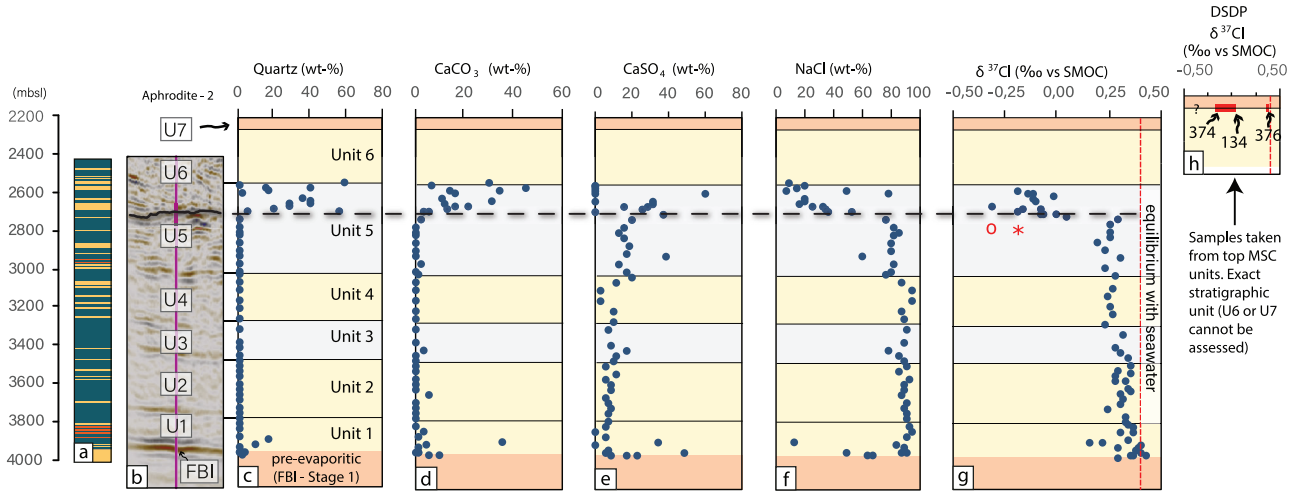

Fig. 2 | Composite log and isotopic results. X-Ray Diffraction (XRD, colour legend as in Fig. 1c) (**a**), mineralogical (**c**–**f**) and chloride isotopic (**g**) composition of cuttings from the Aphrodite 2 hydrocarbon exploration well from the deep Levant Basin, alongside a seismic line crossing the same well (**b**), and chloride isotopic composition (**h**) of halite samples from DSDP sites 134, 374 and 376. Notes: Quartz, $CaCO_3$ (calcite), $CaSO_4$ (anhydrite) and NaCl (halite) are in weight-% of dry sediment, discarding the presence of barite ($BaSO_4$) and sylvite (KCl) which were added to the drilling fluids. FBI stands for Foraminifer Barren Interval[36]. The red dashed line in **g** and **h** represents the equilibrium chlorine stable isotope composition of halite precipitating from seawater. In **c**–**h**, yellow layers (units 1, 2, 4 and 6) are nearly pure halite, gray layers (units 3 and 5) are halite mixed with terrigenous material. In **g**, the red circle and red star represent the $\delta^{37}Cl_{halite}$ data points used to fit the numerical model providing a range of drawdown estimates (Fig. 3). The horizontal black line in **b** is the high-amplitude continuous seismic reflection corresponding to a layer of clastics encased in halite, also shown in Fig. 1d; the dotted black line in c through g represents the vertical position of this reflector relative to the cuttings of core Aphrodite 2. Vertical distance is in meters below sea level. Source data are provided as a Source Data file.

the Aphrodite cuttings (Fig. 2) show that, within seismo-stratigraphic units 1 to 4 and the bottom 360 m of seismo-stratigraphic unit 5 (3943–2700 m depth interval), halite dominates the mineral assemblage (>80 wt-%), with minor (<20 wt-%) amounts of anhydrite ($CaSO_4$) and only trace amounts of $CaCO_3$ and quartz. In the topmost 140 m of seismo-stratigraphic unit 5, the abundance of halite decreases sharply, and that of all the other minerals increases. No samples are available from the well above 2550 m depth, hence no samples are available from unit 6. The drill cuttings also contain sylvite (KCl) and barite ($BaSO_4$) (Supplementary Fig. 1) which were artificially added to the drilling fluids to control their salinity and density, respectively.

Halite grains for Cl-isotope analyses were selected from the drill cuttings under a binocular microscope, excluding grains that contained evident signs of impurities. We cannot exclude, however, that minor amounts of Cl-bearing sylvite (KCl) contributed to the Cl-isotope signature we measured. Mass-balance calculations, however, suggest that the contribution is negligible (see supplementary materials). The $\delta^{37}Cl$ values at the base of the halite layer (0.4 ‰ vs standard mean ocean chloride, hereafter SMOC) are in isotopic equilibrium with oceanic dissolved chloride (0 ‰ vs SMOC) (Fig. 2g). Subsequent halite, forming Levantine basin seismo-stratigraphic units 1 to 4 and the bottom 360 m of seismo-stratigraphic unit 5 (3943–2700 m depth interval), is slightly depleted in ^{37}Cl (average $\delta^{37}Cl = 0.31$ ‰ vs SMOC) compared to equilibrium with global ocean dissolved chloride. We interpret this as reflecting a modest isotope reservoir effect, in which the rate of dissolved chloride sequestration into halite becomes important relative to the influx of chloride from the Atlantic. In the topmost 140 m of seismo-stratigraphic unit 5, $\delta^{37}Cl$ values decrease abruptly, reaching a minimum of −0.30 ‰ vs SMOC at 2630 m depth (Fig. 2g). This is interpreted to reflect a sudden increase in the rate of halite precipitation relative to seawater chloride replenishment.

We also analyzed 9 halite samples from drill cores obtained by drilling the topmost few tens of meters of the deep-basin Mediterranean halite layer during Deep Sea Drilling Project (DSDP) Legs 13 and 42 A from the Florence Rise (Site 376, eastern Mediterranean), Ionian Abyssal Plain (Site 374, eastern Mediterranean) and west Sardinian margin (Site 134, western Mediterranean). A stratigraphic correlation between these sites and the Aphrodite section is not possible, although the position of the DSDP halite samples at the top of the halite body implies that they represent the final stages of the high-salinity evaporite phase of the MSC (Fig. 2). Halite from DSDP samples shows a range of ^{37}Cl depletions from near-equilibrium with oceanic Cl at Site 376 ($0.33 < \delta^{37}Cl$ ‰ vs SMOC < 0.37), to a strong ^{37}Cl-depletion at Site 374 ($-0.14 < \delta^{37}Cl$ ‰ vs SMOC < 0.04). Halite from DSDP Site 134 has intermediate $\delta^{37}Cl$ (0.08 ‰ vs SMOC) (Fig. 2). The ^{37}Cl-depleted isotope signature of halite from DSDP sites cannot be influenced by the composition of drilling fluids, because the halite sub-samples were obtained by mechanically breaking solid halite layers in the DSDP cores, rather than extracted from an admixture of drill cuttings and drilling fluids like for the Aphrodite samples.

Two-phase deposition of the Mediterranean halite layer

We used a numerical model to quantify halite precipitation rates and the extent of sea-level drawdown during the MSC. The model is based on mass balances of water and dissolved ions ($^{35}Cl^-$, $^{37}Cl^-$, Na^+, Mg^{2+}, SO_4^{2-}, Ca^{2+}, K^+ and HCO_3^-) in the western and eastern Mediterranean basins and is forced by the evaporative flux, continental runoff and hydrological restriction at the Gibraltar sill. Evaporation and continental runoff fluxes are based on the Miocene General Circulation Model results of Simon et al.[35]. Starting from initial chemical and hydrologic conditions corresponding to the modern Mediterranean, the model is integrated forwards in time for 20 kyr, after which the hydrological connectivity at Gibraltar is impeded, salinity rises, and evaporitic minerals precipitate. With a salinity-corrected evaporation rate starting at the average value (1 m yr^{-1}) reported in Simon et al.[35] values of continental runoff and hydrological restriction at Gibraltar are found to obtain a good match between simulated and observed[4,25] halite volumes and halite $\delta^{37}Cl$ values. A full description of the numerical model, model forcing and model constraints is given in the supplementary material.

The best fit of the model to the volume and $\delta^{37}Cl$ values of halite (Fig. 3) is obtained if a two-phase hydrological restriction-isolation scenario at Gibraltar is considered. First, the deep-water outflow at Gibraltar is restricted but not blocked, leading to the precipitation of gypsum,

https://doi.org/10.1038/s41467-024-53781-6

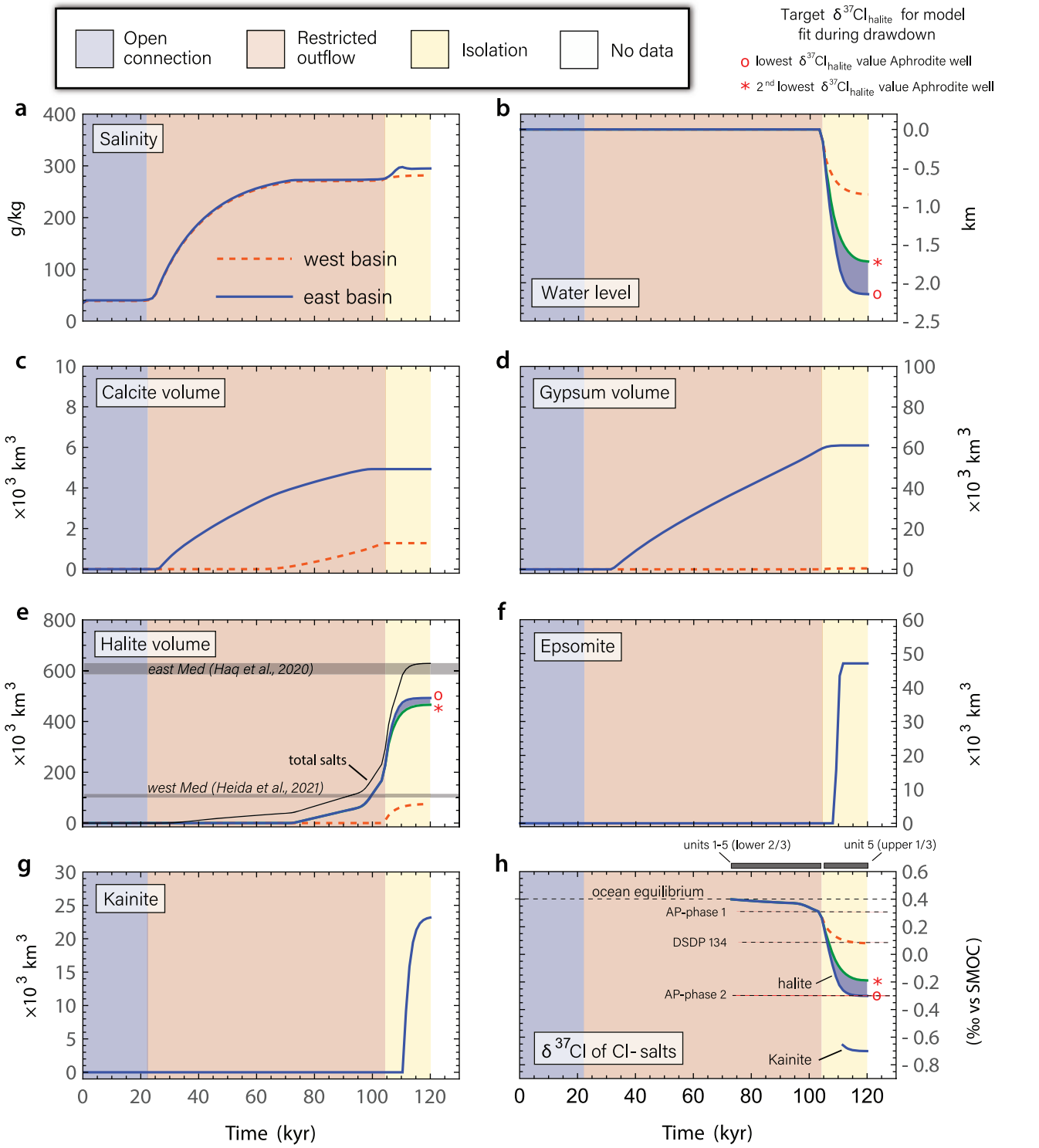

Fig. 3 | Results of the standard model run in the western (orange dashed line) and eastern (solid blue line) Mediterranean basins. a Salinity in g/kg; **b** water level in km; **c** volume (km^3) of precipitated calcite ($CaCO_3$); **d** volume (km^3) of precipitated gypsum ($CaSO_4.2H_2O$); **e** volume (km^3) of precipitated halite (NaCl) and volume (km^3) of total precipitated salts (faint black line); **f** volume (km^3) of precipitated epsomite ($MgSO_4.7H_2O$); **g** volume (km^3) of precipitated kainite ($KClMgSO_4.3H_2O$); **h** δ^{37}Cl of halite and kainite calculated by the model compared to the measured δ^{37}Cl values of halite form Units 1 to the bottom 2/3 of Unit 5 in the Aphrodite-2 core (AP-phase 1), halite from the top 1/3 of Unit 5 in the Aphrodite-2 core (AP-phase 2) and the halite samples at DSDP site 134 (west Sardinia margin). The blue shaded areas represent the ranges of water level (**b**), halite volume (**e**) and $\delta^{37}Cl_{halite}$ (**h**) in the eastern Mediterranean that result if the model is fitted to the lowest measured $\delta^{37}Cl_{halite}$ value (red circle in **h**) or the 2nd lowest $\delta^{37}Cl_{halite}$ value (red star in **h**), by increasing the freshwater continental input in the eastern basin during the drawdown phase (see text); these two $\delta^{37}Cl_{halite}$ data points are highlighted in Fig. 2; the green lines in **b**, **e** and **h** represent model results corresponding to this scenario of increased continental water input.

https://doi.org/10.1038/s41467-024-53781-6

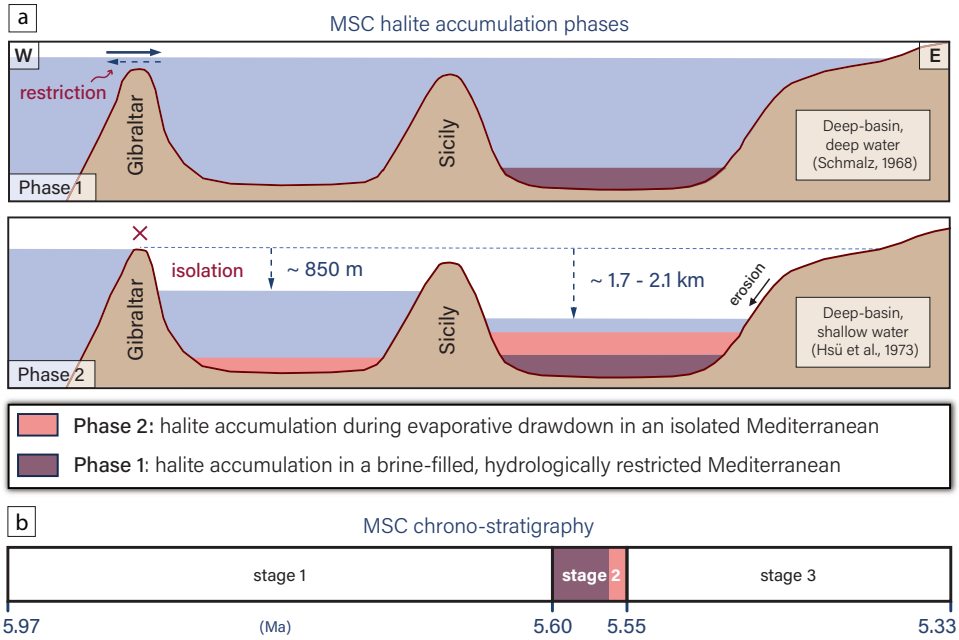

Fig. 4 | Modes of halite accumulation during the Messinian Salinity Crisis deduced from chlorine isotopes of halite and geochemical modeling presented in this work. a Two phases of halite accumulation. During phase 1, halite accumulates in a brine-filled Mediterranean basin that is connected to the Atlantic Ocean but has a hydrologically restricted outflow; during phase 2, the Mediterranean is fully isolated from the Atlantic Ocean and halite accumulates during a major evaporative drawdown event; **b** tentative comparison of the phases of halite accumulation (this work) with the Messinian Salinity Crisis (MSC) chrono-stratigraphic stages after CIESM[38], Roveri et al. (ref. 3) and Ryan[39]. Notes: (i) while we can estimate the duration of the two phases of halite accumulation (**a**), we cannot date them. The tentative correlation with MSC chrono-stratigraphic stages (**b**) is based on the assumption that halite accumulation is restricted to phase 2 of the MSC[3,38,39]; (ii) due to lateral erosion-transport processes, at the Aphrodite 2 site the relative thickness of halite layers is different from the halite volumetric ratios at the scale of the eastern Mediterranean basin.

followed by the precipitation of halite. This halite is characterized by a modest chloride isotope reservoir effect, and decreasing halite $\delta^{37}Cl$ from the value in equilibrium with oceanic dissolved chloride (0.4 ‰ vs SMOC) to the average value measured from seismo-stratigraphic unit 1 to the lower 360 m of unit 5 (0.31 ‰ vs SMOC) (Fig. 3h). In this first phase, lasting about 35 kyr, halite precipitates exclusively in the brine-filled eastern Mediterranean; halite does not precipitate in the western Mediterranean (Fig. 3e) because the brine transferred from the eastern to the western Mediterranean basins across the Sicily sill is in thermodynamic equilibrium with halite, but not supersaturated.

After this first phase, the deep outflow at Gibraltar is blocked and the inflow of Atlantic water into the Mediterranean is stopped, leading to the complete isolation of the Mediterranean Sea from the Atlantic Ocean. As a result, the water level in the entire Mediterranean basin drops until the depth of the Sicily sill is reached, and then continues to fall independently in the western and eastern Mediterranean basins, forced by their respective freshwater budgets (Fig. 3b). The rate of water level fall is very rapid, with 50% of the total drawdown taking place in less than 3.5 kyr, 80% in less than 6 kyr, and the total drawdown attained in less than 10 kyr. Evaporative drawdown causes an abrupt increase in the rate of halite precipitation in the eastern Mediterranean, and to the initiation of halite precipitation in the western Mediterranean (Fig. 3e). The increased halite precipitation rate results in a strong Cl-isotope reservoir effect and an abrupt drop in the $\delta^{37}Cl$ of precipitating halite (Fig. 3h).

In the eastern Mediterranean basin, ~ 40% of the total halite volume formed in the standard model run accumulates in 35 kyr, while the total halite volume accumulates in ~ 50 kyr, in agreement with a "rapid[36]" (~50–60 kyr), rather than a "slow[37]" (~600 kyr), mode of halite accumulation. This time frame is consistent with the widely accepted stratigraphic position of the halite deposit being accumulated during phase 2 of the MSC across the Mediterranean basins (5.60–5.55 Ma; e.g. CIESM[38]; Roveri et al.[3]; Ryan et al.[39]) and, more specifically, in the Levant Basin (Manzi et al.[36]).

After roughly 10 kyr from the beginning of the second phase, the calculated volume of halite in the western (74,900 km^3) and eastern (492,300 km^3) Mediterranean basins approaches the estimates of Heida et al.[25] (110,000–115,000 km^3) and Haq et al.[4] (585,000–657,000 km^3), respectively, while the $\delta^{37}Cl$ of halite in the eastern (−0.30 ‰ vs SMOC) and the western (0.08 ‰ vs SMOC) Mediterranean matches the minimum values measured from the upper 140 m of unit 5 in the Aphrodite well and the top of the salt layer at DSDP Site 374 (both in the eastern Mediterranean) and the value measured in the western Mediterranean at DSDP Site 134, respectively (Fig. 3h). Sensitivity tests (see supplementary material section) show that only a small range of continental runoff values and hydrological restriction at Gibraltar results in a good match of the model to the halite $\delta^{37}Cl$ data and halite volume estimates[4,25], and that within this range, the calculated time to accumulate the halite body and the extent of the drawdown change little.

Our results solve a controversy regarding the mode of halite precipitation – deep basin, deep water[40] vs deep basin shallow water[17] - that is outstanding since the discovery of the deep basin evaporites during DSDP Leg 13[17] (Fig. 4). We show that in the eastern Mediterranean approximately 40% of the halite deposit was formed in a water-filled Mediterranean basin, connected to the Atlantic Ocean by a two-way hydrological exchange, corresponding to the deep-basin, deep-water model[40]. The remaining 60% of the eastern halite deposit was formed by evaporative drawdown of a halite-saturated water body, which is reminiscent of the deep-basin, shallow water model[17], except that halite precipitation takes place during the drawdown, rather than in a deep, desiccated basin after the drawdown took place.

Drawdown of the Mediterranean sea

The water level drawdown we constrain is significant in the western Mediterranean (~850 m), and extreme in the eastern Mediterranean (~2100 m), implying that western and eastern sub-basins lost 43% and

83% of their water volume, respectively. In the eastern Mediterranean, large parts of the continental margins would have been completely desiccated, though the deep Ionian, Herodotus and Antalya basins were still covered by a > 1 km-thick brine layer. Our model also predicts that the drawdown in the eastern Mediterranean resulted in the precipitation of the Mg-K-salts epsomite ($MgSO_4.7H_2O$; 46,700 km^3, Fig. 3f) and kainite ($KMgClSO_4.3H_2O$; 23,200 km^3, Fig. 3g), although Mg-K salts were not detected by XRD in our samples, possibly due to a lateral heterogeneity of brine composition in the eastern Mediterranean, or their dissolution in the drilling fluids or during the washing of drill cuttings. The sequence of precipitation halite-epsomite-kainite is consistent with that observed in seawater evaporation experiments where the minerals are separated from the evaporating brine as they precipitated ("fractional precipitation)[41].

In an attempt to obtain a more conservative estimate of the drawdown extent, we increased the continental freshwater input to the eastern Mediterranean basin in order for the model to reproduce the second-most negative halite $\delta^{37}Cl$ data point measured from cuttings of the Aphrodite well ($\delta^{37}Cl = -0.19$ ‰ vs SMOC; Fig. 2e, star). In these conditions, a more limited drawdown of ~1700 m is calculated (Fig. 3b, green line and star). Taken together these model runs imply that the eastern Mediterranean experienced a large-magnitude drawdown of 1.7–2.1 km during the MSC.

Independent evidence for the occurrence of a sea-level drop and for the subaerial exposure of the basin margins come from the decrease in halite concentration and the peak in Quartz abundance (up to 58 wt-%) in the top 140 m of Unit 5, suggesting significant terrigenous input into the basin during drawdown. The erosion that took place concomitant with the short-lived sea-level drawdown resulted in only a limited accumulation of halite during drawdown at the Aphrodite site (upper 1/3 of Unit 5 above the black horizon traced in the seismic line displayed in Fig. 1d and Fig. 2), compared to the underlying, thick halite layer deposited under a full Mediterranean water column (Units 1–4 and lower 2/3 of Unit 5), leading to a non-linear relation between thickness and volume.

The drawdown of 1.7–2.1 km estimated in this work contrasts with the smaller-magnitude (600 m) drawdown estimated from the restoration of the geomorphological base level of the buried Messinian Nile canyon[9], although the canyon development cannot be precisely dated. If the two estimates refer to the same drawdown event, this implies that the large drawdown was too short-lived to be recorded in the Nile valley geomorphological profile. However, our work shows a complete disconnection of the eastern Mediterranean from the western Mediterranean, implying that, following the first, short-lived, large-scale drawdown, water levels in the eastern Mediterranean would have varied under the influence of an oscillating freshwater budget[35], and of the hydrological connection to the Paratethys drainage system[42]. This hydrological mode, which lasted until the reconnection with the Atlantic via the western Mediterranean, possibly as late as the Zanclean (5.33 Ma)[43,44], leaves ample time for intermediate water levels such as those deduced from the study of topographic profile of the Messinian Nile Canyon[9] to develop.

Consequences of Mediterranean Sea drawdown

Our results have broader implications for the biological, geologic and climatic evolution of the Mediterranean realm, and beyond. In the western Mediterranean sub-basin, the 0.85 km sea-level drawdown we constrain would have resulted in the formation of a land-bridge connecting Africa and Europe through the Betic region and the Balearic Islands. This land bridge would have allowed continental-terrestrial vertebrate fauna to colonize the Balearic islands, a migration that is known to have taken place during the Messinian based on paleontological evidence[45]. A drawdown of 1 km in the western and eastern Mediterranean may have resulted in enough lithospheric unloading to trigger a magmatic pulse in the form of volcanism and dykes in the pan-Mediterranean area at the end of the MSC[46]. Our evidence for drawdowns of ~0.85 km and 1.7–2.1 km in the western and eastern Mediterranean, respectively, make this scenario even more likely. Alongside lithospheric unloading, the huge size of the Mediterranean depression created by MSC water level drawdown - corresponding to a volume loss of 69% of the Mediterranean water body - would have generated planetary-scale climate effects[47], inducing changes in precipitation patterns, a scenario suggested by rainfall proxy data[47].

Methods

X-Ray diffraction (XRD)

The XRD measurements were carried out on an Empyrean diffractometer (@Malvern-Panalytical), equipped with a copper tube and a PIXcel multi-channel detector. The configuration is Bragg-Brentano θ - θ and the sample holder is a spinner. The mineral phases are identified using Highscore plus (@Malvern-Panalytical) software and the ICSD-Panalytical database. Semi-quantitative evaluation of mineral abundances is obtained by scaling the intensities of the principal mineral diffraction peaks to those of reference materials applying reference intensity ratio (RIR) coefficients.

Cl-isotope measurements

We measured the chloride isotope composition of halite grains hand-picked under a binocular microscope, which overwhelmingly reflects that of halite. First, the halite grains were dissolved in distilled water. Then, dissolved Cl ions were precipitated into AgCl and the AgCl converted into CH_3Cl[48–50]. The $\delta^{37}Cl$ of CH_3Cl was measured with a Delta plus XP or Delta V ThermoFisher dual-inlet gas source mass spectrometer. The $\delta^{37}Cl$ compositions are reported in ‰ vs SMOC. The external reproducibility of the internal IPGP standard seawater dissolved chloride (Atlantique 2) was ± 0.025 ‰ (1σ, n = 48); note that this S.D. value is smaller than the size of the $\delta^{37}Cl$ symbols in Fig. 2g.

Numerical model

A full description of the numerical model is provided in the supplementary material.

Data availability

All data generated or analyzed during this study are included in this published article (and its supplementary information). Source data are provided with this paper.

Code availability

The *Mathematica* code used to simulate the evolution of Mediterranean water mass chemistry and chloride isotope composition has been deposited in the Zenodo database (https://zenodo.org/records/13851502) with https://doi.org/10.5281/zenodo.13851502.

References

1. Bethoux, J. P. & Gentili, B. Functioning of the Mediterranean Sea: past and present changes related to freshwater input and climate changes. *J. Mar. Syst.* **20**, 33–47 (1999).
2. Mariotti, A., Struglia, M. V., Zeng, N. & Lau, K.-M. The hydrological cycle in the Mediterranean region and implications for the water budget of the Mediterranean Sea. *J. Clim.* **15**, 1674–1690 (2002).
3. Roveri, M. et al. The Messinian Salinity Crisis: Past and future of a great challenge for marine sciences. *Mar. Geol.* **352**, 25–58 (2014).
4. Haq, B., Gorini, C., Baur, J., Moneron, J. & Rubino, J.-L. Deep Mediterranean's Messinian evaporite giant: how much salt? *Glob. Planet. Change* **184**, 103052 (2020).
5. Chumakov, I. S. Pliocene and Pleistocene deposits of the Nile Valley in Nubia and Upper Egypt (in Russian). Acad. Science, U.S.S.R., *Geol. Institute Trans.*, Moscow, **170**, 5 (1967).

6. Bini, A., Cita, M. B. & Gaetani, M. Southern Alpine lakes—Hypothesis of an erosional origin related to the Messinian entrenchment. *Mar. Geol.* **27**, 271–288 (1978).
7. Barber, P. M. Messinian subaerial erosion of the proto-Nile Delta. *Mar. Geol.* **44**, 253–272 (1981).
8. Clauzon, G. La canyon Messinien du Rhone, une preuve décisive du 'dessicated deep-basin model' (Hsü, Cita et Ryan, 1973). *Bullettin. de. la Soci.été Géologique de. Fr.* **24**, 597–610 (1982).
9. Gvirtzman, Z. et al. Limited Mediterranean sea-level drop during the Messinian salinity crisis inferred from the buried Nile canyon. *Commun. Earth Environ.* **3**, 216 (2022).
10. Ryan, W. B. F. & Cita, M. B. The nature and distribution of Messinian erosional surfaces — Indicators of a several-kilometer-deep Mediterranean in the Miocene. *Mar. Geol.* **27**, 193–230 (1978).
11. Lofi, J. et al. Refining our knowledge of the Messinian salinity crisis records in the offshore domain through multi-site seismic analysis. *Bull. De. La Soc. Geologique De. Fr.* **182**, 163–180 (2011).
12. Lofi, J. et al. Erosional processes and paleo-environmental changes in the Western Gulf of Lions (SW France) during the Messinian Salinity Crisis. *Mar. Geol.* **217**, 1–30 (2005).
13. Urgeles, R. et al. New constraints on the Messinian sealevel drawdown from 3D seismic data of the Ebro Margin, western Mediterranean. *Basin Res.* **23**, 123–145 (2011).
14. Madof, A., Bertoni, C. & Lofi, J. Discovery of vast fluvial deposits provides evidence for drawdown during the late Miocene Messinian salinity crisis. *Geology* **47**, 171–174 (2019).
15. Bertoni, C. & Cartwright, J. A. Major erosion at the end of the Messinian Salinity Crisis: evidence from the Levant Basin, Eastern Mediterranean. *Basin Res.* **19**, 1–18 (2007).
16. Moneron, J., Gvirtzman, Z., Karcz, Z. & Sagy, Y. Discovery of the Messinian Eratosthenes Canyon in the deep Levant Basin. *Glob. Planet. Change* **232**, 104318 (2024).
17. Hsu, K., Ryan, W. & Cita, M. Late Miocene desiccation of Mediterranean. *Nature* **242**, 240–244 (1973).
18. Ryan, W. Quantitative-evaluation of depth of western Mediterranean before, during and after late miocene salinity crisis. *Sedimentology* **23**, 791–813 (1976).
19. Hsü, K. J., Cita, M. B. C. & Ryan, W. B. F. The origin of the Mediterranean evaporites. in *Initial Reports of the Deep Sea Drilling Project* vol. 13 1203–1231 (U.S. Government Printing Office, Washington D.C., 1973).
20. Hsü, K. J. et al. Initial Report of the Deep Sea Drilling Project. *Mediterranean Sea*. vol. 42 (U.S. Government Printing Office, Washington D.C., 1978).
21. Roveri, M. et al. Dense shelf water cascading and Messinian Canyons: A new scenario for the Mediterranean salinity crisis. *Am. J. Sci.* **314**, 751–784 (2014).
22. Hardie, L. A. & Lowenstein, T. K. Did the Mediterranean sea dry out during the miocene? a reassessment of the evaporite evidence from DSDP legs 13 and 42A cores. *J. Sediment. Res.* **74**, 453–461 (2004).
23. Lugli, S., Manzi, V., Roveri, M. & Schreiber, B. C. The deep record of the Messinian salinity crisis: evidence of a non-desiccated Mediterranean sea. *Palaeogeogr., Palaeoclimatol., Palaeoecol.* **433**, 201–218 (2015).
24. Winterberg, S., Picotti, V. & Willett, S. D. Messinian or Pleistocene valley incision within the Southern Alps. *Swiss J. Geosci.* **113**, 7 (2020).
25. Heida, H. et al. Flexural-isostatic reconstruction of the Western Mediterranean during the Messinian Salinity crisis: implications for water level and basin connectivity. *Basin Res.* **34**, 50–80 (2022).
26. Kartveit, K. H., Ulsund, H. B. & Johansen, S. E. Evidence of sea level drawdown at the end of the Messinian Salinity Crisis and seismic investigation of the Nahr Menashe Unit in the northern Levant Basin, offshore Lebanon. *Basin Res.* **31**, 827–840 (2019).
27. Moneron, J. & Gvirtzman, Z. Late Messinian submarine channel systems in the Levant Basin: Challenging the desiccation scenario. *Geology* **50**, 1366–1371 (2022).
28. Blanc, P.-L. Improved modelling of the Messinian Salinity Crisis and conceptual implications. *Palaeogeogr., Palaeoclimatol., Palaeoecol.* **238**, 349–372 (2006).
29. Topper, R. & Meijer, P. A modeling perspective on spatial and temporal variations in Messinian evaporite deposits. *Mar. Geol.* **336**, 44–60 (2013).
30. Roveri, M., Lugli, S., Manzi, V., Gennari, R. & Schreiber, B. C. High-resolution strontium isotope stratigraphy of the Messinian deep Mediterranean basins: Implications for marginal to central basins correlation. *Mar. Geol.* **349**, 113–125 (2014).
31. Topper, R., Flecker, R., Meijer, P. & Wortel, M. A box model of the Late Miocene Mediterranean Sea: Implications from combined Sr-87/Sr-86 and salinity data. *Paleoceanography* **26**, PA3223 (2011).
32. Eggenkamp, H. G. M., Bonifacie, M., Ader, M. & Agrinier, P. Experimental determination of stable chlorine and bromine isotope fractionation during precipitation of salt from a saturated solution. *Chem. Geol.* **433**, 46–56 (2016).
33. Ryan, W. Modeling the magnitude and timing of evaporative drawdown during the Messinian salinity crisis. *Stratigraphy* **5**, 227–243 (2008).
34. Gvirtzman, Z. et al. Intra-Messinian truncation surface in the Levant Basin explained by subaqueous dissolution. *Geology* **45**, 915–918 (2017).
35. Simon, D. et al. Quantifying the Mediterranean freshwater budget throughout the late Miocene: New implications for sapropel formation and the Messinian Salinity Crisis. *Earth Planet. Sci. Lett.* **472**, 25–37 (2017).
36. Manzi, V. et al. Synchronous onset of the Messinian salinity crisis and diachronous evaporite deposition: New evidences from the deep Eastern Mediterranean basin. *Paleogeogr. Paleoclimatol. Paleoecol.* **584**, 110685 (2021).
37. Meilijson, A. et al. Chronology with a pinch of salt: integrated stratigraphy of Messinian evaporites in the deep Eastern Mediterranean reveals long lasting halite deposition during Atlantic connectivity. *Earth Sci. Rev.* **194**, 374–398 (2019).
38. CIESM. *The Messinian Salinity Crisis from Mega Deposits to Microbiology. A Consensus Report*. 91–96 (2008).
39. Ryan, W. B. F. 50th anniversary review of the Mediterranean desiccation hypothesis. *Nuovo Cimento* **46**, 164–291 (2023).
40. Schmalz, R. F. Deep-water evaporite deposition, a genetic model. *Am. Assoc. Pet. Geologists Bull.* **53**, 798–823 (1969).
41. Shalev, N., Lazar, B., Köbberich, M., Halicz, L. & Gavrieli, I. The chemical evolution of brine and Mg-K-salts along the course of extreme evaporation of seawater – An experimental study. *Geochimica et. Cosmochimica Acta* **241**, 164–179 (2018).
42. Marzocchi, A., Flecker, R., Baak, C. G. C., van, Lunt, D. J. & Krijgsman, W. Mediterranean outflow pump: An alternative mechanism for the Lago-mare and the end of the Messinian Salinity Crisis. *Geology* **44**, 523–526 (2016).
43. Van Dijk, G. et al. A terminal Messinian flooding of the Mediterranean evidenced by contouritic deposits on Sicily. *Sedimentology* **70**, 1195–1223 (2023).
44. Spatola, D. et al. A single-stage megaflood at the termination of the Messinian salinity crisis: Geophysical and modelling evidence from the eastern Mediterranean Basin. *Mar. Geol.* **430**, 106337 (2020).
45. Mas, G. et al. Terrestrial colonization of the Balearic Islands: New evidence for the Mediterranean sea-level drawdown during the Messinian Salinity Crisis. *Geology* **46**, 527–530 (2018).
46. Sternai, P. et al. Magmatic pulse driven by sea-level changes associated with the Messinian salinity crisis. *Nat. Geosci.* **10**, 783–787 (2017).
47. Murphy, L., Kirk-Davidoff, D., Mahowald, N. & Otto-Bliesner, B. A numerical study of the climate response to lowered Mediterranean Sea level during the Messinian Salinity Crisis. *Palaeogeogr. Palaeoclimatol. Palaeoecol.* **279**, 41–59 (2009).

48. Kaufmann, R., Long, A. & Davis, S. Natural chlorine isotope variations. *Nature* **309**, 338–340 (1984).
49. Godon, A. et al. A cross calibration of chlorine isotopic measurements and suitability of seawater as the international reference material. **207**, 1–12 (2004).
50. Eggenkamp, H. G. M. *The Geochemistry of chlorine isotopes* (Utrecht University, 1994).

Acknowledgements

This study was supported by the European Union's Horizon 2020 research and innovation program under the Marie Skłodowska-Curie grant agreement number 765256 SALTGIANT and by the CNRS via IODP-France through a post-cruise grant. We acknowledge Modi'in Energy and Pelagic partnership for their permission to release data related to the well Aprodite-2. We thank HIS Markit for providing us the Kingdom academic licenses for seismic interpretation.

Author contributions

G.A. designed the study. G.A., L.G., G.B. and P.A. carried out the chloride isotope measurements of halite and interpreted the data. G.A. developed the numerical model and applied it to interpret the halite chloride isotope data with input from I.G., R.E. and J.M. G.A., J.M., L.G., A.C., I.G., G.B., P.A., R.E. and Z.G. contributed to the final manuscript preparation.

Competing interests

The authors declare no competing interests.

Additional information

Supplementary information The online version contains supplementary material available at https://doi.org/10.1038/s41467-024-53781-6.

Correspondence and requests for materials should be addressed to G. Aloisi.

Peer review information *Nature Communications* thanks Jeremiah Bernau, Neil Mitchell and Mebrahtu Weldeghebriel for their contribution to the peer review of this work. A peer review file is available.